Carbon 250 (2026) 121254

Contents lists available at ScienceDirect

Carbon

journal homepage: www.elsevier.com/locate/carbon

Graphene oxide nanosheet trehalose-assisted lyophilization with enhanced stability and facile aqueous reconstitution for biopharmaceutical use

Gloria Garcia-Ortega [a,b], Neus Lozano [a,b], Kostas Kostarelos [a,b,c,d,*]

[a] Nanomedicine Lab, Catalan Institute of Nanoscience and Nanotechnology (ICN2), CSIC and BIST, Campus UAB, 08193, Barcelona, Spain
[b] Institute of Neuroscience, Universitat Autònoma de Barcelona, 08913, Barcelona, Spain
[c] ICREA, Pg. Lluís Companys 23, Barcelona, Spain
[d] Centre for Nanotechnology in Medicine, Faculty of Biology, Medicine & Health, The University of Manchester, Manchester, UK

ARTICLE INFO

Keywords:
Lyophilization
Freeze-drying
Trehalose
Lyoprotectant
Nanoparticle formulation
Pharmaceutical applications
Drug delivery
Flexible electronics
Graphene-based composites
Storage stability
Solid-state processability

ABSTRACT

Graphene oxide (GO) has emerged as a nanomaterial of considerable interest owing to its unique physicochemical properties, including excellent water dispersibility, ease of functionalization, and favorable biocompatibility and safety profile. These features position GO as a promising and tunable platform for a wide range of technological and biomedical applications. Accordingly, as GO-based systems continue to advance toward real-world applications, considerations around long-term storage and stability are gaining relevance. Lyophilization is a widely adopted strategy to preserve the structural and functional integrity of nanomaterials to be reconstituted on demand, yet GO suspensions exhibited poor stability upon reconstitution following lyophilization. We present a simple and effective method using trehalose (T) as a lyoprotectant to stabilize GO during lyophilization. The resulting dried GO + T formulations exhibit improved reconstitution behavior at physiological pH, and characterization confirms the preservation of the nanosheet structural integrity. More specifically, such approach can enable the long-term storage of GO, facilitating its further development as a biopharmaceutical agent.

1. Introduction

Graphene oxide (GO) has stood out as a structurally versatile two-dimensional nanomaterial over the past decades. It possesses a honeycomb structure composed of aromatic (sp^2) and aliphatic (sp^3) domains. Its basal planes and edges are functionalized with oxygen-containing groups such as carboxylic, epoxy, or hydroxyl moieties, which impart broad aqueous dispersibility to the nanomaterial. The unique structural and chemical properties of GO have enabled diverse applications, including sensing, energy technologies and environmental remediation platforms [1–7]. Among these, in the biomedical field GO has gained significant attention, supported by extensive studies on biodegradability, biocompatibility, and biodistribution; all key parameters that determine its safety profile and will allow its integration into healthcare and medical technologies [8–14].

We have previously developed 'medical-grade' GO synthesized via a modified Hummer's method, with well-defined lateral dimensions, free from endotoxins and structural or chemical impurities that has been clinically used in a first-in-human cardiopulmonary acute response study [15,16]. Such GO nanosheets can be readily functionalized through both covalent and non-covalent strategies, positioning this 2D nanomaterial as a highly tunable platform for diverse biomedical applications, including drug delivery, diagnostics, tissue engineering and implantable electronics [17–22]. Such versatility highlights the potential of GO for translation into clinical applications.

To achieve market success, nanomaterials-based formulations must meet several critical criteria, with quality and stability being foremost [23]. A key requirement is an extended shelf-life, which significantly impacts cost-effectiveness, environmental sustainability and supply chain logistics [24,25]. Long-term preservation also plays a critical role in maintaining the safety and efficacy of the formulation by preventing microbial contamination and chemical degradation [26]. A widely adopted strategy to improve shelf-life is solvent removal, yielding in a dry, solid formulation that can be readily reconstituted on demand. However, preserving GO suspensions for extended periods can pose a significant challenges, due to its reliance on electrostatic stabilization [27]. To support long-term storage and facilitate clinical translation and commercialization, this study aimed to develop and evaluate a protocol for producing dried, ready-to-use GO at physiologically relevant pH. Although dehydration of GO under vacuum has been reported, it leads to

* Corresponding author. Nanomedicine Lab, Catalan Institute of Nanoscience and Nanotechnology (ICN2), CSIC and BIST, Campus UAB, 08193, Barcelona, Spain
E-mail address: kostas.kostarelos@icn2.cat (K. Kostarelos).

https://doi.org/10.1016/j.carbon.2026.121254
Received 22 August 2025; Received in revised form 7 January 2026; Accepted 8 January 2026
Available online 8 January 2026

irreversible crosslinking that compromises aqueous stability and hinders reconstitution [28]. Other drying techniques, such as lyophilization and spray drying, have been applied for fabricating or post-processing GO-based nanomaterials, yielding powders, porous structures, nanoscrolls and crumpled spheres, among others [20,29–35]. However, these methods typically induce structural and chemical alterations, making it impossible to recover its native colloidal stability upon rehydration. Consequently, no drying approach has been explored to specifically preserve thin GO nanosheets in a stable, readily reconstitutable form.

Lyophilization, or freeze-drying, is one of the most employed techniques in the pharmaceutical industry for preserving labile formulations [36]. However, the process can exert significant stress on macromolecules and nanomaterials, potentially leading to structural collapse or degradation. To mitigate these effects, lyoprotectants, excipients added during formulation, are used to stabilize and protect sensitive components throughout the freezing and drying stages. These agents help prevent or reduce the formation of damaging ice crystals, which are a primary source of structural disruption during lyophilization [36–38]. The selection of a lyoprotectant depends on the specific physicochemical properties and requirements of the system. Common lyoprotectants include sugars (e.g., dextrose, sucrose), sugar-alcohols (e.g., mannitol, sorbitol), proteins (e.g., albumin) or surfactants (e.g., polyvinylpyrrolidone) [24,39]. Among these, non-reducing disaccharides like sucrose and trehalose (T) are widely used due to their ability to maintain an amorphous state upon drying, a key property for effective lyopreservation of proteins and other macromolecules [40,41].

Advantages of T over sucrose, include greater chemical inertness, due to the highly stable glycosidic bond that makes it less prone to hydrolysis. It also exhibits high viscosity and kosmotropic effects, both of which contribute to its protective capabilities during lyophilization. Notably, T presents the highest glass transition temperature (Tg) amongst disaccharides (~106–120 °C depending on the source), allowing lyophilized formulations to be stored at room temperature without compromising stability, as molecular mobility remains negligible well below Tg [42–45]. T is reported to stabilize macromolecular structures through at least two primary mechanisms: (i) water replacement capability, whereby T substitutes water molecules to form a stabilizing environment around the macromolecule through hydrogen bonding that limits motion, and/or (ii) vitrification or physical immobilization within a glassy matrix, that forms upon dehydration entrapping the material [41,43,44,46–48]. Furthermore, T is non-toxic and is approved as an excipient of widespread use in food, cosmetic, and pharmaceutical industries, including approved formulations of monoclonal antibody therapeutics, oral tablets and vaccines [49,50].

This work aimed to combine T-based lyophilization, as a well-established method for safeguarding macromolecular structures in dry form with advances in graphene-based 2D nanomaterials development, offering a path toward the usability and commercialization of GO-based technologies. While lyophilization has been extensively applied to various nanomaterials using established lyoprotectants and protocols, this study presents, to the best of our knowledge, the first application of this methodology to a GO nanosheet suspension with the explicit goal of achieving long-term storage followed by facile reconstitution in water. T was employed as a lyoprotectant to preserve colloidal stability and physicochemical integrity during drying and rehydration process.

2. Experimental

Materials and reagents: GO was produced from graphitic powder, as previously reported in the group, by a modified Hummer's method, Table S1 [16]. Commercial GO was acquired from Graphenea (GO in water 0.4 % wt, pH 2.2–2.5). Anhydrous D-(+)-Trehalose (99 % HPLC purity) and anthrone ACS (10H-anthracen-9-ona) were purchased from Thermo Scientific Chemicals. Sigma-Aldrich (Merck, Spain) was the provider for the rest of the chemicals used during the work. The water for injection employed for GO preparation and further studies was acquired from Grifols. The Amicon Ultra-4 Centrifugal Filter units (100 kDa MWCO) were purchased from Merk-Milipore (UFC810024).

Preparation of GO and GO + Trehalose: In all cases GO was adjusted to pH 7.2 to 7.6 using NaOH 100 mM solution to promote the biocompatibility, stability, and reliable behavior of GO in biological conditions. T was added to GO + T solutions at 5 and 10 %, which corresponded to 1:50 and 1:100 mass ratios (wt:wt) and then diluted to reach to 1 mg/ml GO concentration. In each step the solution was homogenized, and after water addition, the solutions were submitted to mild orbital shaking (1 G) at room temperature and finally stabilized for 1 h prior to use. The pH was recorded during all the steps using a pH meter FiveEasy™ FP20 with Mettler Toledo™ pH Electrode InLab Ultra-Micro-ISM calibrated every 24 h with technical buffers (pH 4.1, 7.00 and 9.21) from Fisher Scientific.

Lyophilization and reconstitution protocol: The desired volume of the GO + T 5 % or 10 % solution was directly placed into a glass vial and immediately frozen using liquid nitrogen. The frozen GO sample was placed on the lyophilization flask and attached to a port of the manifold to connect the flask to the drying chamber. Then, the vacuum valve was slowly opened, letting the sample lyophilized below 0.01 mBar for over 24 h. Each lyophile was resuspended to the initial water volume to keep the GO concentration. During the reconstitution step, a first 15 s vortexing at high speed was conducted, followed by 5 min sonication in a bath sonicator. In each step the sample was characterized by DLS.

Free trehalose separation and quantification: To evaluate the extent of T adsorption onto GO, free T was separated by a centrifugal filter (Amicon®, CTA 4 mL, 3 kDa MWCO), for which each unit was filled with T control, neutral-GO, or GO + T suspensions. The unit was centrifuged for 4 cycles at 4000 G for 10 min at 20 °C. When each filtration cycle finished, the filtrate was collected and the volume on the centrifugal filter was adjusted to the initial volume for the subsequent cycle. The corresponding T controls were also submitted to the same procedure to verify no retainment of T on the membrane. T was quantified by the Anthrone assay for sugar quantification. In this colorimetric assay, carbohydrates are dehydrated by concentrated sulfuric acid to furfural, which reacts with anthrone to generate a blue-green dye with maximum absorbance at 620 nm. For the measurement, all the solutions were diluted 500 times and 200 μL of the solution was mixed with 800 μL of Anthrone reagent. The mixture was homogenized and placed in an ice bath for 5 min. Then, the solution was allowed to equilibrate to room temperature and measured by UV–Vis. A calibration curve of T was performed following the same protocol.

Characterizations. UV–Vis: Absorbance spectra were measured at Evolution 201 UV–Vis spectrophotometer from Thermo Scientific in the range on 200–800 nm at room temperature using a Hellma QS Quartz cuvette. Calibration curve for T/anthrone solutions were recorded by measuring the maximum absorbance (620 nm) at increasing T concentrations (from 0.5 to 20 %, diluted 500 times), with the corresponding water-H_2SO_3 solution as a reference. GO and GO + T samples were measured at a GO concentration of 20 μg/mL.

Dynamic Light Scattering: Hydrodynamic diameter, PDI and zeta potential were measured on a Zeta-sizer Nano ZS (Malvern Instrument). Samples were measured before lyophilization and after the lyophile resuspension at a GO concentration of 20 μg/mL in disposable capillary cells using 1 mL of solution. Water was selected as dispersant and material refractive index and absorption were set to 2.00 and 0.300, respectively.

Atomic Force Microscope: AFM micrographs were recorded in an Agilent 5500 AFM/SPM microscope with a scanning probe with Tap300 Al-G tips (BugdetSensors) with a nominal force of 40 N/m and a frequency of 300 kHz in combination with PicoScan5 Software. Sample preparation was performed by drop casting 20 μL of 0.01 % poly-L-lysine solution (Sigma-Aldrich) onto a cleaved mica disc. Then, the surface was washed with 1 mL of water, and 20 μL of 100 μg/mL of GO solution were cast onto the mica. Finally, the surface was washed again and dried at room temperature for at least 12 h. AFM images were recorded at 5 × 5

μm and processed with Gwyddion software (version 2.56).

Scanning Electron Microscopy: STEM micrographs were recorded in a Magellan 400L field emission microscope (Oxford instruments) with an Everhart-Thornley detector for secondary electrons at ICN2 Electron Microscopy Unit. For sample preparation, 20 μL of GO solution at 100 μg/mL were dropped cast onto Ultrathin C on Lacey C films (Ted Pella) and then bloated to remove the excess. The process was repeated 4 times and then samples was left to dry overnight. The conditions employed were a beam current of 100 pA and an acceleration voltage of 20 kV.

Optical Microscopy: was recorded using Eclipse LV100D (Nikon) microscope, at 50X magnification, using NIS-Elements F 3.0 software. Samples were prepared drop casting 20 μL of GO solution (20 μg/mL) onto a glass slide and let dry overnight.

Osmolality: Solution osmolality was measured in an osmometer Osmomat 030, calibrated with standards of 300 mOs/kg. 50 μL of each sample were measured in triplicate, and the measurement was repeated 3 times.

Raman: Spectra were recorded with a Witec Ramanspectrometer equipped with a red laser ($\lambda = 633$ nm). The laser was focused on the sample using a 50X magnification objective. Spectra were recorded using an acquisition time of 25 s and 5 accumulations using a power of 0.4 mW. GO was drop cast into a glass slide at a concentration of 50 μg/mL in triplicate. The I_D/I_G were calculated based on measurements taken from five replicates of each sample.

X-ray Photoemission Spectroscopy: XPS spectra were recorded on a Phoibos 150 (SPECS GmbH) electron spectrometer coupled with a hemispherical analyzer, under ultrahigh-vacuum conditions and with Al Kα (hv = 1486.74 eV) X-Ray source was used to the measurements acquisition. The measurements were performed at the ICN2 Photoemission Spectroscopy Facility. Charge effects were removed by taking the C 1s line from adventitious carbon at 284.6 eV. Samples were prepared by drop casting 20 μL (0.5–1 mg/mL GO) until total coverage on the top of a 5 × 5 mm Si Water (Ted Pella). For data treatment CasaXPS software was used.

X-ray diffraction: XRD spectra were collected on Malvern PANalytical X'Pert Pro MPD diffractometer in the 2θ scan range from 5 to 60° with an X-ray source of a ceramic X-ray tube with Cu Kα anode (λ = 1.540 Å) and the x'Celerator solid-state detector at the ICN2 XRD Facility. Solutions were drop cast (20 μL) on a Si holder and dried at room temperature until full coverage of the holder centre. Lyophilized solids were measured in solid state. Spectra were analyzed using X'Pert HighScore version 2.2.3.

Fourier Transform Infrared Spectroscopy: Lyophilized solids were measured using Fourier Transform infrared attenuated total reflectance (FTIR-ATR) on a Tensor 27/PMA 50 FT-IR spectrometer (Bruker) with a resolution of 4 cm^{-1} and a scan range of 3750 to 600 cm^{-1} at ICN2 Molecular Spectroscopy and Optical Microscopy Facility.

Surface tension: was recorded with a DSA25S (Krüss) equipped with a high-speed camera with a resolution of 1920 × 1200 px and an automatic Software-controlled dispenser and titling stage. Solutions were measured at 1 mg/mL of GO concentration.

Differential scanning calorimetry: DSC measurements were carried out on a TA Instruments Discovery Series DSC25 equipped with a Refrigerated Cooling System 90 (RCS90). Samples were sealed in aluminium pans and analyzed under a nitrogen purge at a heating/cooling rate of 10 °C/min from 30 °C to 250 °C. For each sample, four full cycles were performed and the third run was analyzed.

Thermogravimetric Analysis. The residual water content of the samples exposed to storage conditions were measured by thermogravimetric analyses (TGA) performed on a PerkinElmer TGA 8000 instrument. Experiments were conducted with a heating ramp of 10 °C/min from 30 to 600 °C under nitrogen flow (50 mL/min).

All the spectra were analyzed using OriginPro 2018 (version b9.5.0.193). Some schematics included in the figures of this manuscript were created with BioRender.com.

3. Results and discussion

3.1. Overcoming graphene oxide (GO) instability during lyophilization with trehalose

Reconstitution of lyophilized GO at physiologically relevant pH revealed significant colloidal instability upon reconstitution. Despite vigorous vortexing (15 s) and sonication (5 min), the resuspended material exhibited visible precipitation (Fig. 1A). Optical microscope confirmed the presence of large aggregates while electron microscope showed the loss of nanosheets individuality. Moreover, the GO suspension was measured using dynamic light scattering (DLS), but the results evidenced hydrodynamic diameters over 1 μm, beyond the detection limit of the instrument, and with high polydispersity index (PDI) values (data not shown). These results indicated that lyophilizing GO without lyoprotectant compromises its colloidal integrity upon rehydration.

To improve GO reconstitution following lyophilization, T was selected as a lyoprotectant. Effective lyoprotectants typically maintain an amorphous state during drying, a critical property for preserving colloidal stability [26]. Among them, sugars are widely used due to their ability to stabilize nanomaterials with minimal impact on osmolality, an essential consideration for parenteral formulations [51]. T is a widely used excipient across biotechnology and food industries due to its exceptional stabilizing capabilities. Its high-water solubility (~50 g/100 mL) and elevated Tg enable the formation of a stable amorphous matrix during lyophilization. Moreover, its non-reducing nature and robust glycosidic linkage confer resistance to degradation under a range of pH and temperature conditions. Unlike other disaccharides, T lacks intra-molecular hydrogen bonding, enhancing its ability to form stabilizing hydrogen bonds with suspended nanomaterials during lyophilization [48].

The optimal lyoprotectant concentration depends on formulation requirements. In pharmaceutical applications, concentrations typically range from 1 to 10 % (w/v) [47,52–54]. Accordingly, in this study, T was incorporated into GO suspensions at concentrations of 5 % and 10 % (w/v), selected based on literature precedence and lyoprotectant efficacy. The preparation steps followed for the resulting formulations, hereinafter denoted GO + T 5 % and GO + T 10 %, are illustrated in Fig. S1A.

T was incorporated into GO suspensions, and after homogenization (Fig. S1A), comprehensive physicochemical characterization was performed to assess the impact of T on GO suspensions. Size, morphology, surface chemistry, and surface tension analyses (Figure S1 B-F) revealed no significant changes relative to GO. Dynamic light scattering (DLS) (Fig. S1B) and zeta potential (Fig. S1C) measurements, showed comparable values across all samples. It is important to note that DLS values may not be accurate for non-spherical geometry nanoparticles such as GO, but they remain useful for monitoring relative changes. Electron microscopy (Fig. S1D) confirmed that the morphology of GO nanosheets remained unchanged upon T addition. Raman spectroscopy further supported structural integrity: G and D bands (~1595 cm^{-1} and ~1335 cm^{-1}, respectively) and the I_D/I_G ratio remained consistent, with no shifts or spectral distortions observed (Fig. S1E). Additionally, surface tension values (Fig. S1F) were similar across samples and within the range for water, indicating no macroscopic alterations on the suspension due to T.

To evaluate the potential interaction of T with the GO nanosheet surface, indirect quantification of unbound T was performed by measuring the amount of free sugar remaining in solution. GO samples were processed using ultrafiltration columns, where the free T was collected at the bottom of the column. Filtration cycles were carried out with free T and GO used as controls (Fig. S2). GO retention was confirmed in all GO-containing samples, with negligible GO loss observed (Fig. S2A). In contrast, T readily passes through the membrane, as demonstrated by its complete recovery at the bottom of the column (Fig. S2B). However, due to the low UV–Vis absorbance of T and spectral

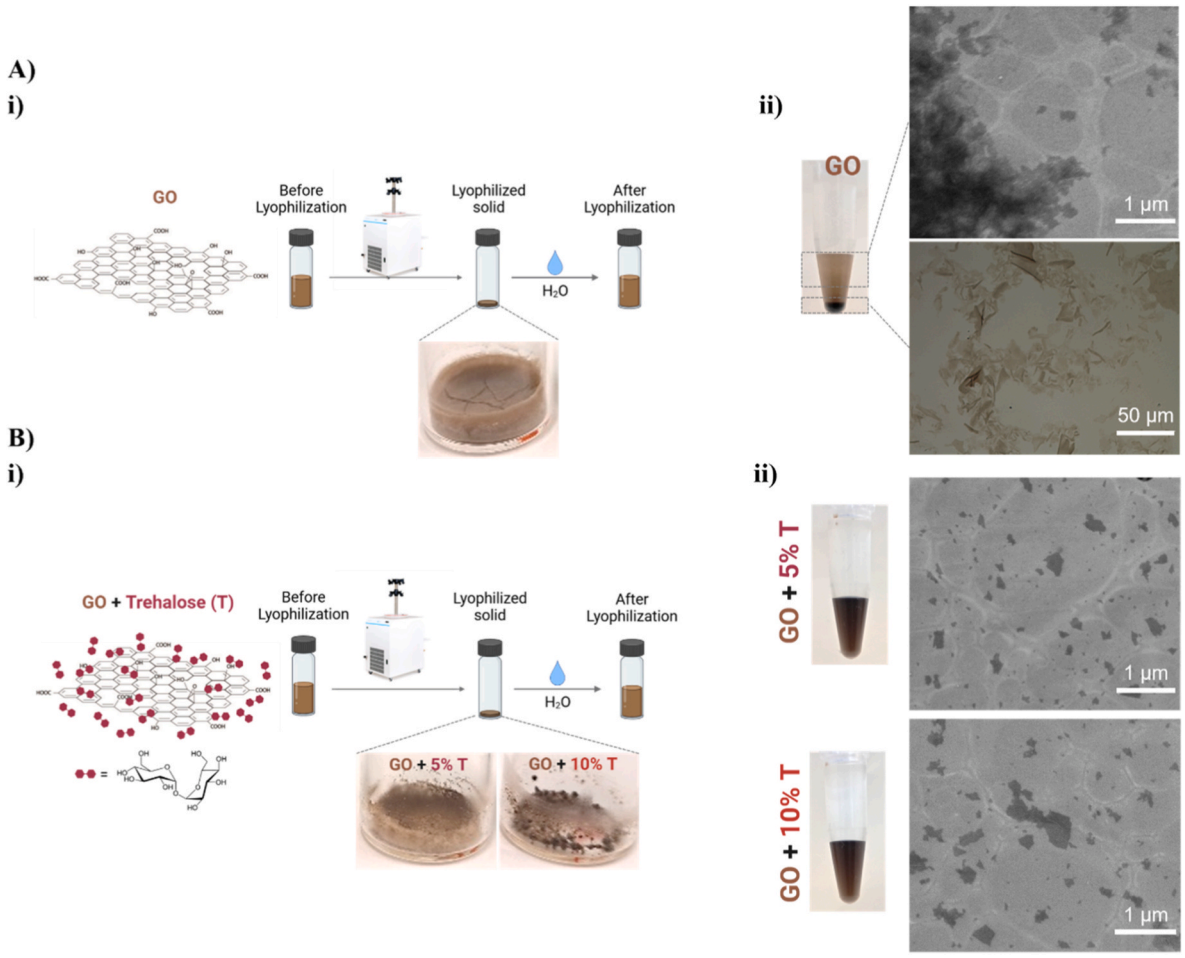

Fig. 1. Graphene oxide (GO) nanosheet lyophilization in (A) absence and (B) presence of trehalose. (Ai) GO lyophilization in the absence of trehalose (T) results in instability and aggregation of the reconstituted nanosheets, as observed (Aii) by electron and optical microscopy. (Bi) Illustration of lyophilization process of GO using T as the lyoprotectant at two distinct concentrations (5 and 10 %); and (Bii) electron microscopy confirming the GO nanosheets individuality after lyophilization and reconstitution in water.

overlap with GO signals, direct quantification was not feasible. Instead, we employed the Anthrone assay, a colorimetric method in which carbohydrates are dehydrated with sulfuric acid to form furfural, which reacts with Anthrone rendering a blue/green detectable chromophore at 620 nm (Fig. S3). Results showed minimal interaction between T and GO, with free T recovery values of 100 and 94 % for GO + T 5 % and GO + T 10 %, respectively, indicating only residual binding of T to the GO surface (Fig. S3B). These findings are consistent with the absence of major physicochemical changes observed by DLS, Raman and surface tension measurements.

Upon lyophilization of T-containing GO samples, reconstitution yielded visually homogeneous suspensions (Fig. 1B–ii). Thus, to assess the preservation of colloidal stability, DLS was used to monitor the hydrodynamic diameter of GO suspensions before and after lyophilization (Fig. 2A,B). As this parameter is highly sensitive to nanosheet aggregation, its retention is considered a reliable indicator of lyophilization efficiency. The results demonstrated that both GO + T 5 % and GO + T 10 % samples successfully recovered their initial hydrodynamic diameters after reconstitution, even with brief vortexing (15 s). The corresponding DLS profiles showed Gaussian peaks closely matching the original distributions, indicating the absence of aggregation. Ratios of post-to pre-lyophilization diameters are commonly used to assess lyophilization efficiency, where values close to 1 indicate good preservation of the nanomaterials, and values above 1 suggest aggregation [47]. As listed in Table S2, both T-containing GO were consistently below 1, indicating a slight size reduction rather than aggregation. The polydispersity index (PDI), which reflects alterations in the particle hydrodynamic diameter distribution, remained stable at ~ 0.38 across all samples (Fig. 2C), further supporting the maintenance of a uniform nanosheet population. Zeta potential values (Fig. 2D) also remained consistent before and after lyophilization, indicating that the surface properties of GO were preserved. Together, these DLS-derived parameters confirm that T effectively stabilizes GO nanosheets during freeze-drying and reconstitution: the colloidal integrity was maintained across both T concentrations, and recovery was achieved with minimal agitation.

Further characterizations of the reconstituted solutions were performed to ensure the preservation of other physical parameters on the nanosheets and the GO suspension. UV–Vis spectroscopy before and after lyophilization revealed clear differences between the formulations (Fig. 2E,F). All samples initially showed a characteristic absorbance peak at 230 nm and a shoulder at 300 nm, corresponding to π–π* transitions of C═C and n–π* transitions of C═O groups, respectively. After reconstitution, the GO + T 5 % and GO + T 10 % samples exhibited absorbance profiles comparable to their pre-lyophilization states, indicating no loss or aggregation of the material (Fig. 2F). In contrast, GO showed a marked decrease in absorbance, consistent with precipitation or the formation of larger aggregates with altered optical properties (Fig. 2E). A thorough characterization, focusing on alterations in the functionalization degree of the GO surface post-lyophilization, was conducted using XPS. The analysis (Fig. 2G) was used to assess the C/O of the material before and after lyophilization. The initial C/O ratio for

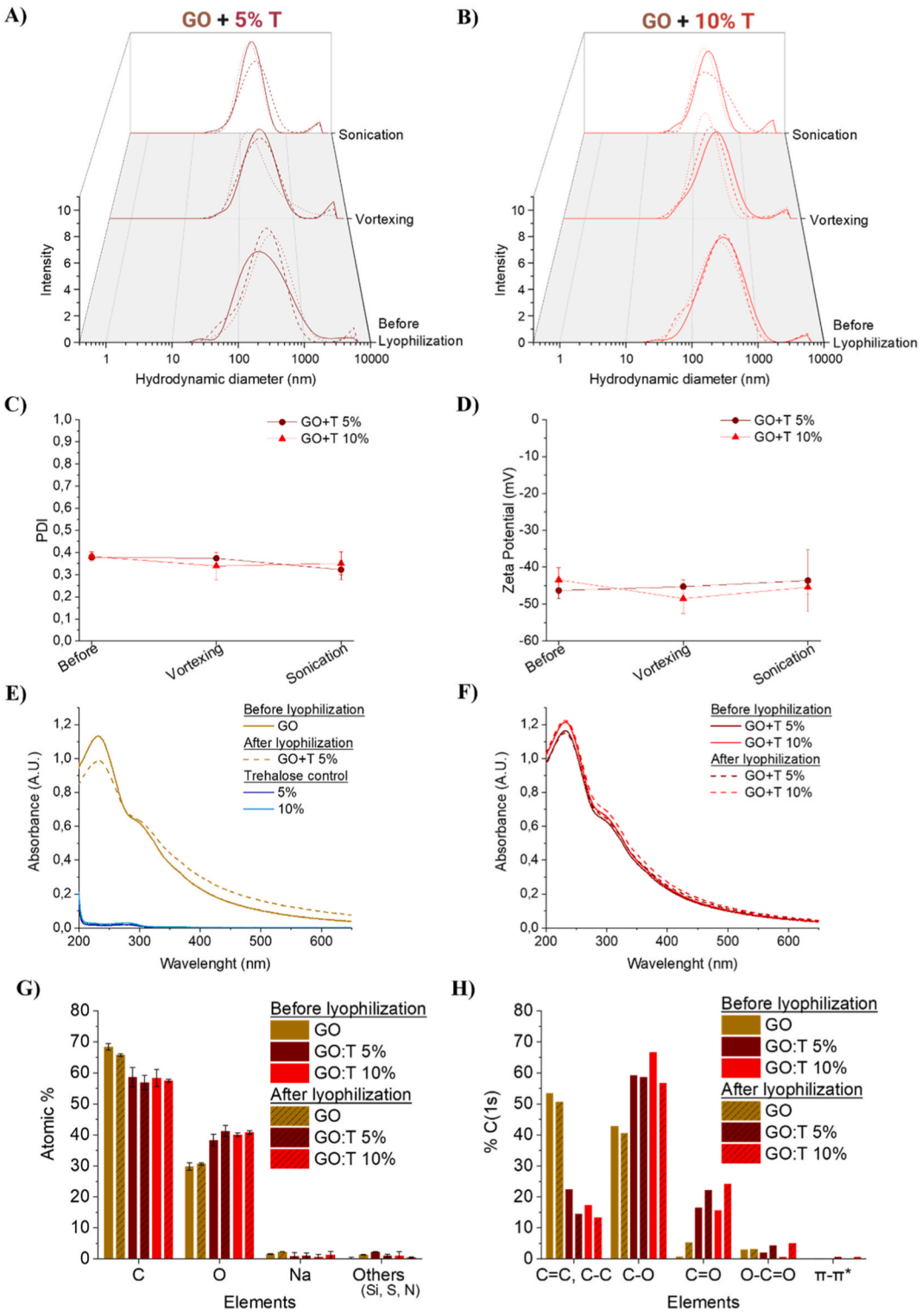

Fig. 2. DLS plots showing the hydrodynamic diameter before lyophilization and after reconstitution of GO with T of (A) GO + T 5 % and (B) GO + T 10 %. Each line in the graph represents and individual replicate. Average (C) PDI and (D) zeta potential values before and after lyophilization (n = 3). Data for GO in the absence of T are not shown, as the particle size exceeded the measurable range of the instrument due to extensive aggregation. UV–Vis absorbance spectra of (E) GO and T controls and (F) GO + T samples, showing complete GO reconstitution in trehalose-containing formulations in contrast to the loss of GO absorbance in the absence of T. (G) XPS survey analysis comparing the surface chemistry of GO-based samples before and after lyophilization, showing the relative atomic percentages of key surface elements (C, O, Na, and trace elements such as Si, S, N). The carbon and oxygen content remain relatively consistent, indicating the chemical stability of GO during the lyophilization process. Slight variations in carbon and oxygen levels reflect the presence of T. The Si signal originates from the substrate used for measurement. (H) Deconvolution of XPS C (1s) peaks to understand differences in the functional groups before and after lyophilization and reconstitution. All samples were reconstituted in water prior to analysis (n = 2).

GO was 2.3, in agreement with previously reported C/O ratios for GO [16]. As expected, the addition of T slightly decreased the C/O ratio to 1.5 for both T concentrations, consistent with the oxygen-rich structure of the sugar. After reconstitution, all samples exhibited a negligible decrease in C/O ratios, yielding 2.1 for GO and 1.4 for the T-containing formulations.

The chemical changes that could be occurring to GO were quantitatively verified by XPS C 1s deconvolution (Fig. S4) analysis summarized in Fig. 2H. The GO control sample, dried without T, exhibited a net decrease in the stabilizing C–O component concurrently with a relative increase in the C═O component. This chemical rearrangement could be indicative of instability during the lyophilization process in the absence of the lyoprotectant. The GO + T formulations also showed changes: C 1s deconvolution of GO + T 5 % showed a minor absolute loss of the crucial C–O component (only 0.5 %) that increased up to 9.8 % in GO + T 10 %. The decrease in the graphitic (C═C and C–C) components and the increase in the C═O component is attributed to a dilution effect stemming from the incorporation of the T molecule itself. As T is a C–*O*-rich polyol, its carbon signal increases the total relative contribution of oxygenated carbon components in the final dried film, necessarily decreasing the relative percentage of the non-oxygenated C═C and C–C backbone. The larger C–O variation for the GO + T 10 % sample is potentially associated to the loss of loosely associated T molecules during lyophilization, rather than a reduction of the protected GO backed up by the fact that any other technique showed changes on the GO behavior reconstitution and the easy reconstitution of GO in the presence of T.

Another critical parameter in pharmaceutical formulations is pH, as maintaining a physiological pH can enhance biocompatibility, improve drug absorption, and reduce degradation. A quasi-neutral pH is also compatible with most parenteral routes and is often recommended to minimize pain, irritation and tissue damage, particularly for subcutaneous injections [55]. For these reasons, pH was monitored throughout the lyophilization process per triplicate. Pre- and post-lyophilization the values remained stable, with initial values of 7.6 ± 0.2, 7.4 ± 0.2, and 7.5 ± 0.3, and post-process values of 7.7 ± 0.3, 7.6 ± 0.1, and 7.4 ± 0.1, for GO, GO + T 5 % and GO + T 10 %, respectively. Likewise, osmolality, a measure of solute concentration in a liquid, is a critical parameter on parenteral formulations, as affects safety, tolerability, biodistribution, and regulatory compliance. Therefore, osmolality was measured throughout the lyophilization process. Upon the addition of T to GO, values of 121.3 ± 2.1 and 254.0 ± 2.0 mOs/Kg for 5 and 10 % T were measured, respectively. These values remained stable after reconstitution, with osmolality measurements of 126.2 ± 6.1 mOs/kg for GO + T 5 % and 249.0 ± 8.5 mOs/kg for GO + T 10 %. These values were consistent with T controls (119.7 ± 2.5 and 251.7 ± 2.1 mOs/Kg for 5 and 10 % of T), confirming that T is primarily accounted for osmolality, and further supported by the near-zero osmolality of GO being 0 ± 1.7 mOs/Kg. Both GO + T formulations were hypotonic (<300 mOs/kg), with the 10 % formulation falling within the acceptable range for parenteral and oral administration [51,56,57].

To unequivocally assess the preservation of the GO + T nanosheets morphology, Atomic Force Microscopy (AFM) was performed before and after lyophilization. As shown in Fig. 3, the AFM micrographs demonstrated that the GO nanosheets retained its morphology and individuality, with no evidence of aggregation at either of the employed concentrations. Furthermore, height profile analysis confirmed that the nanosheet thickness remained constant after reconstitution, with values ranging from 1.1 to 1.5 nm, consistent with monolayer GO and indicating that residual T bound to the GO surface does not compromise its quality after lyophilization.

3.2. *Elucidating the mechanism of trehalose lyoprotection in graphene oxide*

Fourier-transform infrared spectroscopy (FTIR) was employed to evaluate possible interactions between GO and T in the lyophilized samples (Fig. S5). The spectra of GO + T formulations (5 % and 10 %) resembled a combination of the individual GO and T spectra, showing characteristic features from both components. No major shifts were observed in the O–H, C═O, or C═C stretching regions, suggesting the absence of strong interactions between GO and T. The reduced intensity of these signals in the T-containing formulations is likely due to spectral overlap from T. Additional minor bands corresponding to C–H and C–O vibrations were consistent across all samples.

X-ray diffraction (XRD) was employed to evaluate the crystalline structure of the components before and during the solid lyophilized state. Prior to freeze-drying, GO exhibited its characteristic broad diffraction peak around 10° (Fig. S6A), consistent with its layered structure. In contrast, T displayed sharp, intense diffraction peaks characteristic of a crystalline structure (Fig. S6B). In the GO + T formulations, the crystalline signal from T dominated the XRD patterns, masking the broad GO peak (Fig. S6C and D). Upon freezing, T is known to transition into an amorphous glassy state that inhibits ice crystal formation and protects the structural integrity of labile components. To confirm this transition, XRD analyses were performed on the lyophilized solids of the GO + T samples. As shown in Fig. 4A,B, the resulting spectra exhibited fully amorphous profiles, consistent with the protective effect of T during lyophilization. In our study, the amorphous nature of T in the dried GO formulation, its lack of adsorption onto the nanosheets, and the absence of broadening in the O–H stretching band (~3300 cm^{-1}) indicate minimal specific interactions between T and GO, which aligns with the vitrification mechanism. These findings suggest that T does not chemically modify GO, but rather stabilizes it through a physical mechanism.

In this context, T stabilizes the nanomaterial by forming a highly viscous, glass-like matrix during freeze-drying, which physically entraps and immobilizes the GO nanosheets, preserving its structural integrity [48]. This protective effect is closely associated with the glass transition temperature (Tg) of T. Below Tg, the T matrix remains in a brittle, glassy state, that minimizes molecular mobility and effectively immobilizes the GO nanosheets, preventing aggregation or degradation. As the temperature approaches or exceeds Tg, the matrix would transition into a rubbery, more fluid-like state, leading to increased molecular mobility and reducing its structural protection. Therefore, maintaining storage conditions well below Tg is critical to ensure long-term stabilization of GO through vitrification.

To evaluate the physical state of T in the formulation the Tg was determined by Differential Scanning Calorimetry (DSC). Two samples were employed, a freshly lyophilized GO + T 10 % and a sample stored in their dried lyophilized state (under dark conditions) for four months to also consider the effect of long-term storage in T's state. The DSC thermograms (Fig. 4C) revealed a Tg of 123 °C for the freshly lyophilized sample and 120 °C for the stored sample. For comparison, the lyophilized T solution exhibited a Tg of 123.5 °C, showing only minor differences from the GO-containing samples but slightly exceeding literature values (106–120 °C), likely due to its low residual water content [45]. Indeed, literature reports that a 1 % change in water content can have plasticizing effects, reducing Tg by up to 5 °C [58]. Thermogravimetric analysis (TGA) confirmed low levels of residual moisture across all samples in Fig. 4D. Weight losses attributed to the release of loosely bound water (up to 120 °C) were 1.01 % for the fresh sample and 2.59 % for the 4 months stored sample. When the analysis temperature increased to account for the release of tightly bound water (150 °C), the cumulative mass losses remained low and highly comparable: 2.97 and 2.78 %, respectively. The corresponding mass losses for T control were 2.33 % (at 120 °C) and 2.55 % (at 150 °C), that could explain the minor differences of Tg measured. Overall, the residual moisture levels in the freeze-dried formulations, with total mass losses consistently below 3 %, are considered acceptable according to established guidelines for pharmaceutical and biological lyophilized products [59].

Overall, the high Tg values indicate a rigid, low-mobility matrix that preserves nanosheet dispersion and prevents chemical degradation

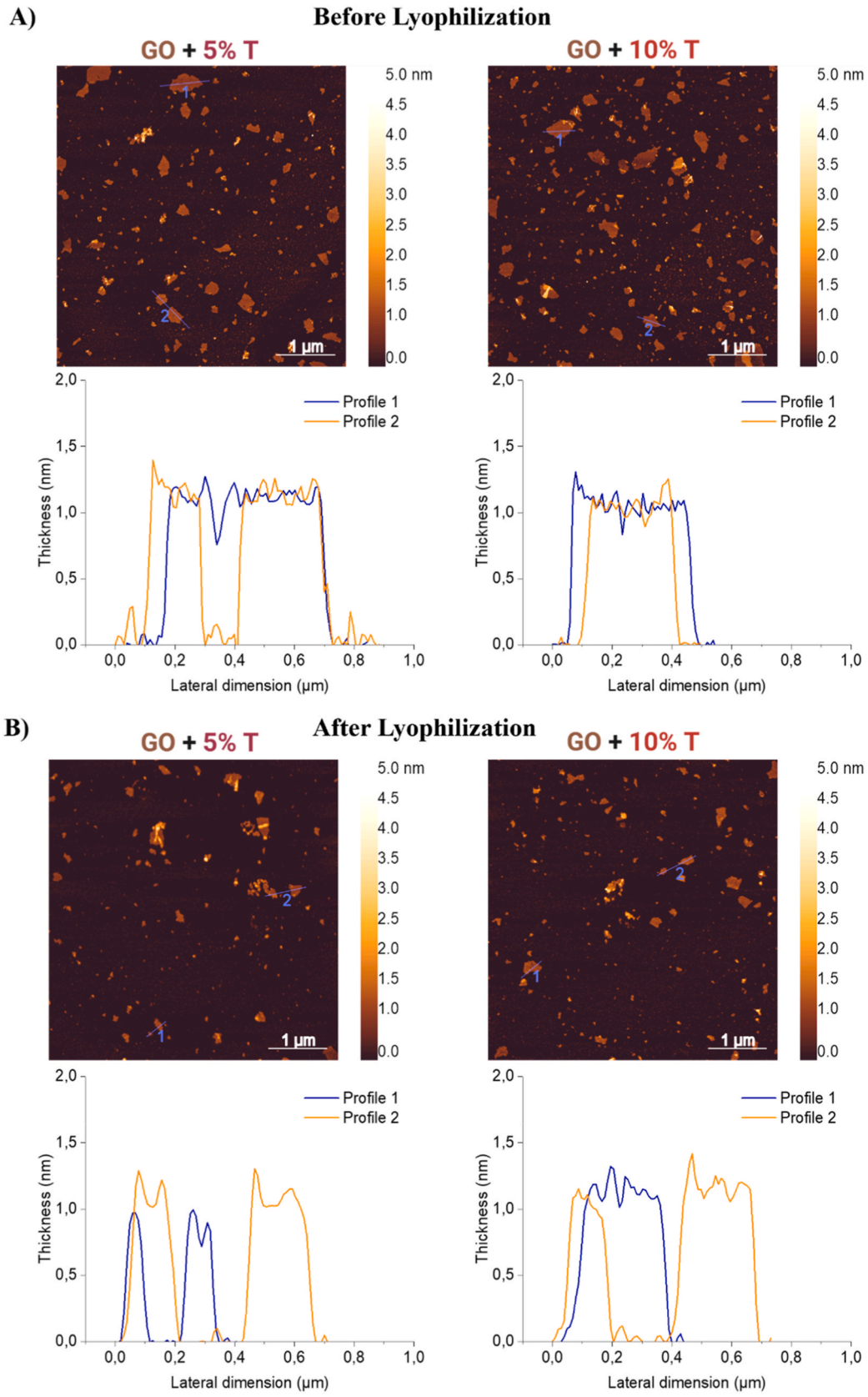

Fig. 3. AFM micrographs showing the morphology and thickness of GO + T nanosheets (A) before and (B) after lyophilization, for formulations containing 5 % (left) and 10 % T (right). The images display nanosheets morphology and the thickness profiles after its reconstitution in water.

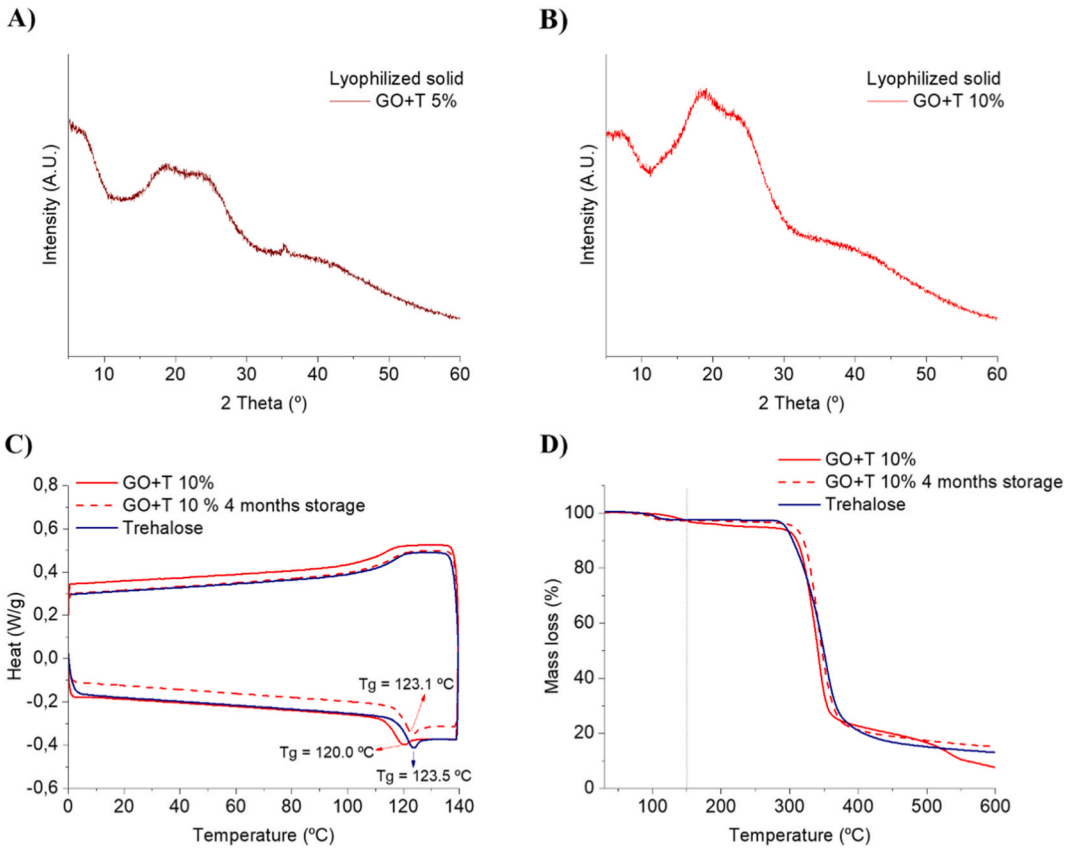

Fig. 4. Characterization of lyophilized dried state of GO + T samples. XRD patterns of lyophilized solids of (A) GO + T 5 % and (B) GO + T 10 %. T appears amorphous post-lyophilization, in contrast to its original crystalline form (see Fig S6). (C) DSC and (D) TGA showing the glass transition temperature (Tg) and moisture content of fresh and 4-month-stored GO + T 10 % samples. The Tg value for each sample is indicated in the graph. The TGA of all the samples exhibited mass losses below 3 % measured at 150 °C (dotted line), indicating minimal changes in residual moisture during storage. The consistent Tg values well above the storage temperature and the low residual moisture confirmed vitrification-based stabilization, where T remains glassy and immobilizes GO for enhanced stability.

during long-term storage. The consistent Tg across samples confirms that T remains in an amorphous glassy state well above the storage temperature (~20 °C), supporting vitrification as the dominant stabilization mechanism for GO. The minor Tg variations observed are consistent with residual moisture effects and do not suggest any loss of vitrification. Collectively, these findings demonstrate that T maintains its amorphous glassy structure during storage, ensuring a stable microenvironment that effectively preserves the structural integrity of GO.

3.3. From powder to shelf: solid-state processability and storage of graphene oxide (GO)

To assess the applicability of GO lyophilization for storage and processing, we explored the effects of powdering the dried solids prior to reconstitution. Remarkably, grinding the lyophilized solids had no detrimental impact on the reconstitution, as demonstrated by consistent hydrodynamic diameters observed in both GO + T 5 % and GO + T 10 % (Fig. S7). This capacity to powder the lyophilized solid without compromising colloidal integrity significantly expands the material's handling and processing options, offering potential for integration into solid-state formulations or composites. Furthermore, to confirm the method versatility, the protocol was applied to GO from a commercial source, which initially presented a larger hydrodynamic diameter than the in-house produced material. As shown in Fig. S8, commercial GO samples containing T fully recovered its original hydrodynamic diameters distribution after a brief 15-s vortexing step. Mild sonication further reduced particle size, consistent with the behavior of thin GO nanosheets. Conversely, commercial GO samples lacking T, reflected a substantial increase in hydrodynamic diameter and aggregation, though, these samples were excluded from the DLS analysis due to their poor re-dispersibility.

The long-term stability of the lyophilized solids was further validated through storage at room temperature in dark for 4 months and 1 year. Upon reconstitution after 4 months, T-containing formulations (GO + T 5 % and GO + T 10 %) retained key colloidal characteristics, including hydrodynamic diameter, PDI, and zeta potential when compared to their pre-lyophilization states, as seen in Fig. 5A, B, C and D, respectively. After one year of storage, a clear distinction emerged between the two T concentrations. A 10 % T content was necessary to maintain colloidal stability, as the 5 % formulation exhibited early signs of aggregation, as supported by DLS measurements (Fig. 5A). These observations were corroborated by morphological analyses, EM (Fig. 5E) and AFM (Fig. 5F). Both confirmed the preservation of nanosheet structure and height profiles for the GO + T 10 % sample, while the 5 % formulation showed evidence of increased aggregation and thicker nanosheets on the height profiles. Our hypothesis is that the 10 % T concentration provides a more robust protective environment, particularly critical for room-temperature storage, due to the higher availability of T molecules to effectively immobilize GO nanosheets over extended periods. However, for shorter-term storage, both concentrations performed comparably, suggesting that the optimal T percentage can be tailored according to formulation-specific requirements such as osmolality, route of administration, viscosity, storage conditions, or regulatory constraints.

Together, these results demonstrate that T effectively stabilizes GO across different sources, enables long-term dry-storage, and mechanical processing, while keeping facile hydration. This establishes a broadly applicable framework for the preservation and deployment of GO, paving the way for its integration into a wide range of advanced material

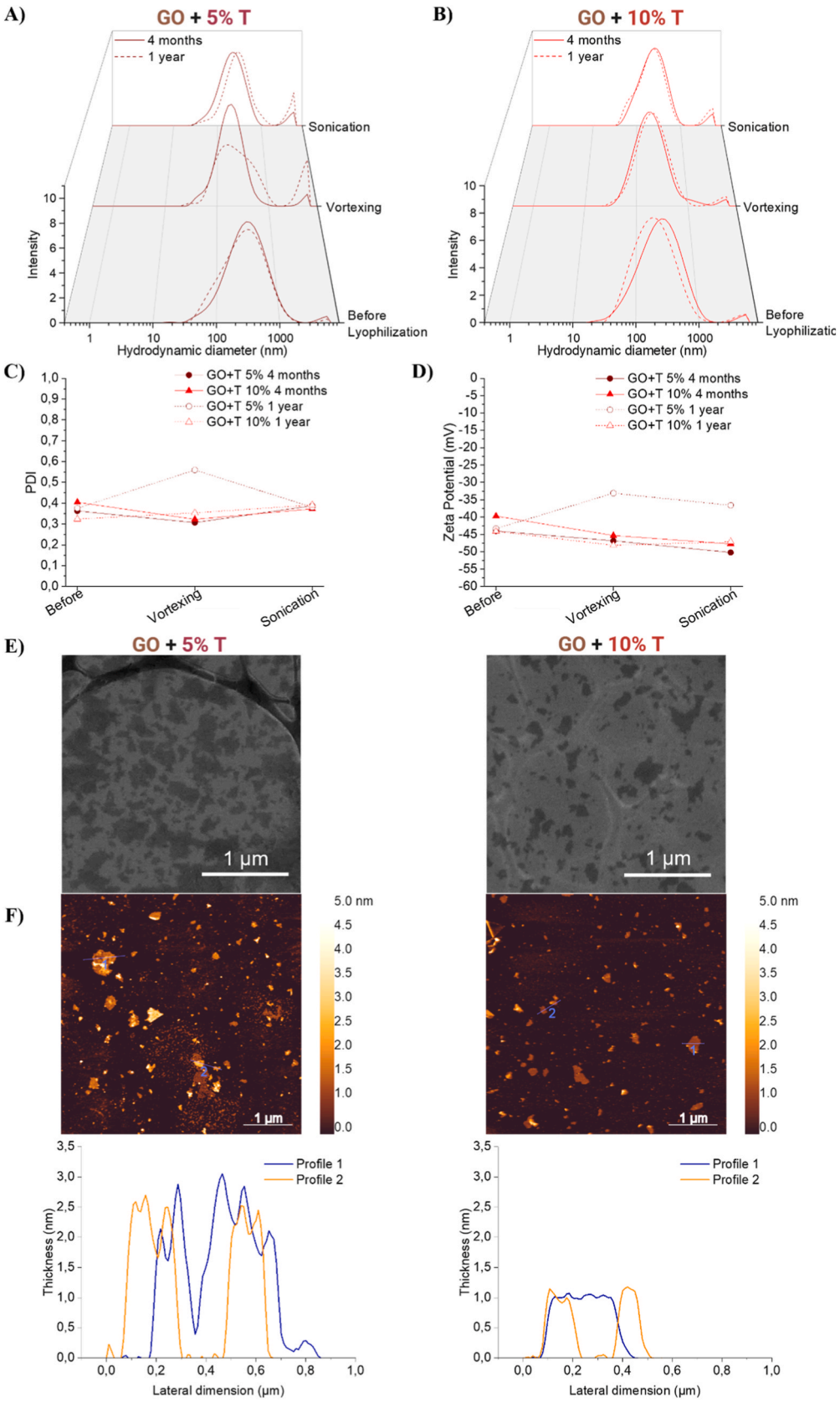

Fig. 5. The reconstitution of GO after four months (solid line) and 1 year (slashed line) of storage at room temperature, depicted by: (A, B) hydrodynamic diameter, (C) PDI, and (D) zeta potential for GO + T 5 % and GO + T 10 %. GO alone (without T) is not shown as the hydrodynamic diameter measured exceeded the validation range of DLS. (E) Electron microscope and (F) AFM micrographs, with corresponding height profiles, of GO + T 5 % (left) and GO + T 10 % (right) samples reconstituted 1 year after storage.

systems. While reconstitutable GO holds great promise in pharmaceutical and biomedical fields, where GO can serve as a carrier for drugs, genes, or imaging agents, this approach also broadens its utility across technological fields. In areas where solid-state processability, reproducibility, and long-term storage are critical prerequisites for scalability, the ability to stabilize GO in a dry, functional and readily rehydratable form is particularly valuable.

4. Conclusions

This study showed that the incorporation of T as lyoprotectant, enables effective lyophilization of thin GO nanosheet suspensions, preserving its physicochemical integrity for up to one year. In the absence of lyoprotectant, GO becomes unstable upon lyophilization, limiting its potential for long-term dry solid storage, a form widely used in pharmaceuticals to extend shelf life. The incorporation of T at 5 % and 10 % concentrations did not alter key physicochemical characteristics of the GO sheets, including their Raman signature, morphology and thickness. The lyophilized formulations containing T allowed rapid and complete reconstitution into a stable colloidal suspension (within just 15 s of vortexing) without compromising the physicochemical integrity of GO or suspension parameters such as surface tension, pH, and osmolality. The unchanged thicknesses, and the lack of strong or specific interactions between T and GO suggest that T is not strongly adsorbed onto the GO surface but rather remains primarily dispersed in the aqueous phase. Furthermore, the amorphous glassy state observed in the lyophilized solid, confirmed by XRD and DSC, with Tg values well above the storage temperature and low residual moisture levels (<3 %), supports a stabilization mechanism based on physical immobilization by vitrification, rather than chemical interaction. Collectively, these results confirm that T provides a stable vitrified matrix that preserves the structural integrity and stability of GO over time.

The method remained effective for storage durations of 4 months and 1 year, confirmed by DLS and EM, with 10 % T best maintaining stability at the longest time point. For shorter-term storage, both T concentrations performed comparably, and the choice can be guided by other formulation constraints.

Importantly, the resulting solid cakes can be processed making this approach highly compatible with scalable manufacturing and solid-state integration. The protocol was also validated using commercially available GO batches, suggesting potential applicability across different graphene-based materials. Future work should focus on refining the lyophilization cycle to improve cake morphology and reproducibility, particularly for industrial-scale applications. Moreover, while the approach could be compatible with sterile environments, such as lyophilization under aseptic conditions, additional validation would be necessary for manufacturing-scale production. Altogether, the choice of T represents a purposeful step towards bridging materials science and pharmaceutical technology. The proposed simple and effective strategy demonstrates potential as a practical platform for the solid-state handling and long-term storage of GO, particularly in contexts relevant to pharmaceutical technology.

CRediT authorship contribution statement

Gloria Garcia-Ortega: Writing – original draft, Validation, Methodology, Investigation, Data curation, Conceptualization. **Neus Lozano:** Writing – review & editing, Supervision, Project administration, Methodology. **Kostas Kostarelos:** Writing – review & editing, Supervision, Methodology, Funding acquisition, Conceptualization.

Declaration of generative AI and AI-assisted technologies in the writing process

During the preparation of this work the authors used ChatGPT, an AI language model developed by OpenAI, in order to improve grammar and language clarity during the editing of this manuscript. After using this tool/service, the author(s) reviewed and edited the content as needed and take full responsibility for the content of the publication.

Funding

The authors would like to thank the European Union Horizon 2020 Research and Innovation Programme under Grant Agreement no. 881603 (Graphene Flagship Core 3) to financially support this project. The ICN2 is supported by the CERCA programme/Generalitat de Catalunya. The ICN2 is supported by the Severo Ochoa Centres of Excellence programme, Grant CEX2021-001214-S, funded by MCIU/AEI/10.13039.501100011033.

Declaration of competing interest

The authors declare that they have no known competing financial interests or personal relationships that could have appeared to influence the work reported in this paper.

Acknowledgements

The authors would like to acknowledge the ICN2 Advanced Electronic Materials and Devices Group, led by Prof. Jose A. Garrido for providing access to Raman equipment in their laboratory. We also like to thank Dr. Nerea Murillo-Cremaes and Dr. Tommaso Battisti for their contribution on the synthesis and characterization of the specific GO batch used in this study. Additionally, we thank Prof. Daniel Maspoch and Dr. Arnau Carné for providing access to DSC and TGA equipments, and especially to Dr. Fran Sanchez-Férez assistance on these experiments.

Appendix A. Supplementary data

Supplementary data to this article can be found online at https://doi.org/10.1016/j.carbon.2026.121254.

References

[1] T. Lin, X. Ren, X. Wen, A. Karton, V. Quintano, R. Joshi, Membrane based In-situ reduction of graphene oxide for electrochemical supercapacitor application, Carbon N. Y. 224 (2024) 119053, https://doi.org/10.1016/j.carbon.2024.119053.
[2] Y. Tian, Z. Yu, L. Cao, X.L. Zhang, C. Sun, D.-W. Wang, Graphene oxide: an emerging electromaterial for energy storage and conversion, J. Energy Chem. 55 (2021) 323–344, https://doi.org/10.1016/j.jechem.2020.07.006.
[3] H. Ahmad, M. Fan, D. Hui, Graphene oxide incorporated functional materials: a review, Composites, Part B 145 (2018) 270–280, https://doi.org/10.1016/j.compositesb.2018.02.006.
[4] D. Lei, Q. Zhang, N. Liu, T. Su, L. Wang, Z. Ren, Z. Zhang, J. Su, Y. Gao, Self-powered graphene oxide humidity sensor based on potentiometric humidity transduction mechanism, Adv. Funct. Mater. 32 (2022) 1–12, https://doi.org/10.1002/adfm.202107330.
[5] S. Dayana Priyadharshini, S. Manikandan, R. Kiruthiga, U. Rednam, P.S. Babu, R. Subbaiya, N. Karmegam, W. Kim, M. Govarthanan, Graphene oxide-based nanomaterials for the treatment of pollutants in the aquatic environment: recent trends and perspectives – a review, Environ. Pollut. 306 (2022) 119377, https://doi.org/10.1016/j.envpol.2022.119377.
[6] M. Sun, J. Li, Graphene oxide membranes: functional structures, preparation and environmental applications, Nano Today 20 (2018) 121–137, https://doi.org/10.1016/j.nantod.2018.04.007.
[7] G. Yildiz, M. Bolton-Warberg, F. Awaja, Graphene and graphene oxide for biosensing: general properties and the effects of graphene ripples, Acta Biomater. 131 (2021) 62–79, https://doi.org/10.1016/j.actbio.2021.06.047.
[8] C. Chung, Y.K. Kim, D. Shin, S.R. Ryoo, B.H. Hong, D.H. Min, Biomedical applications of graphene and graphene oxide, Acc. Chem. Res. 46 (2013) 2211–2224, https://doi.org/10.1021/ar300159f.
[9] V. Palmieri, F. Bugli, M. Cacaci, G. Perini, F. De Maio, G. Delogu, R. Torelli, C. Conti, M. Sanguinetti, M. De Spirito, R. Zanoni, M. Papi, Graphene oxide coatings prevent Candida Albicans biofilm formation with a controlled release of curcumin-loaded nanocomposites, Nanomedicine 13 (2018) 2867–2879, https://doi.org/10.2217/nnm-2018-0183.
[10] H. Zhang, R. He, Y. Niu, F. Han, J. Li, X. Zhang, F. Xu, Graphene-enabled wearable sensors for healthcare monitoring, Biosens. Bioelectron. 197 (2022) 113777, https://doi.org/10.1016/j.bios.2021.113777.

[11] I. de Lázaro, P. Sharp, C. Gurcan, A. Ceylan, M. Stylianou, T. Kisby, Y. Chen, S. Vranic, K. Barr, H. Taheri, A. Ozen, C. Bussy, A. Yilmazer, K. Kostarelos, Deep tissue translocation of graphene oxide sheets in human glioblastoma 3D spheroids and an orthotopic xenograft model, Adv. Ther. 4 (2021) 1–15, https://doi.org/10.1002/adtp.202000109.
[12] A. Ruiz, M.A. Lucherelli, D. Murera, D. Lamon, C. Ménard-Moyon, A. Bianco, Toxicological evaluation of highly water dispersible few-layer graphene in vivo, Carbon N. Y. 170 (2020) 347–360, https://doi.org/10.1016/j.carbon.2020.08.023.
[13] B. Fadeel, C. Bussy, S. Merino, E. Vázquez, E. Flahaut, F. Mouchet, L. Evariste, L. Gauthier, A.J. Koivisto, U. Vogel, C. Martín, L.G. Delogu, T. Buerki-Thurnherr, P. Wick, D. Beloin-Saint-Pierre, R. Hischier, M. Pelin, F. Candotto Carniel, M. Tretiach, F. Cesca, F. Benfenati, D. Scaini, L. Ballerini, K. Kostarelos, M. Prato, A. Bianco, Safety assessment of graphene-based materials: Focus on human health and the environment, ACS Nano 12 (2018) 10582–10620, https://doi.org/10.1021/acsnano.8b04758.
[14] J.P.M. Andrews, S.S. Joshi, E. Tzolos, M.B. Syed, H. Cuthbert, L.E. Crica, N. Lozano, E. Okwelogu, J.B. Raftis, L. Bruce, C.A. Poland, R. Duffin, P.H.B. Fokkens, A.J. F. Boere, D.L.A.C. Leseman, I.L. Megson, P.D. Whitfield, K. Ziegler, S. Tammireddy, M. Hadjidemetriou, C. Bussy, F.R. Cassee, D.E. Newby, K. Kostarelos, M.R. Miller, First-in-human controlled inhalation of thin graphene oxide nanosheets to study acute cardiorespiratory responses, Nat. Nanotechnol. 19 (2024) 705–714, https://doi.org/10.1038/s41565-023-01572-3.
[15] D.A. Jasim, N. Lozano, K. Kostarelos, Synthesis of few-layered, high-purity graphene oxide sheets from different graphite sources for biology, 2D Mater. 3 (2016) 014006, https://doi.org/10.1088/2053-1583/3/1/014006.
[16] A.F. Rodrigues, L. Newman, N. Lozano, S.P. Mukherjee, B. Fadeel, C. Bussy, K. Kostarelos, A blueprint for the synthesis and characterisation of thin graphene oxide with controlled lateral dimensions for biomedicine, 2D Mater. 5 (2018) 035020, https://doi.org/10.1088/2053-1583/aac05c.
[17] A.M. Itoo, S.L. Vemula, M.T. Gupta, M.V. Giram, S.A. Kumar, B. Ghosh, S. Biswas, Multifunctional graphene oxide nanoparticles for drug delivery in cancer, J. Contr. Release 350 (2022) 26–59, https://doi.org/10.1016/j.jconrel.2022.08.011.
[18] R. Imani, F. Mohabatpour, F. Mostafavi, Graphene-based nano-carrier modifications for gene delivery applications, Carbon N. Y. 140 (2018) 569–591, https://doi.org/10.1016/j.carbon.2018.09.019.
[19] M. Stylianou, T. Kisby, D. Despotopoulou, H. Parker, A. Thawley, K. Arashvand, N. Lozano, A.S. MacDonald, K. Kostarelos, Engineering the glioblastoma microenvironment using TLR7/8 agonist-complexed graphene oxide nanosheets, Cell Rep. Phys. Sci. 6 (2025) 102342, https://doi.org/10.1016/j.xcrp.2024.102342.
[20] I. Zare, M. Mirshafiei, B. Kheilnezhad, B.F. Far, M. Hassanpour, E. Pishbin, S. S. Eftekhar Vaghefi, F. Yazdian, H. Rashedi, A. Hasan, X. Wang, M. Adeli, P. Makvandi, Hydrogel-integrated graphene superstructures for tissue engineering: from periodontal to neural regeneration, Carbon N. Y. 223 (2024) 118970, https://doi.org/10.1016/j.carbon.2024.118970.
[21] M. Dong, P. Chen, K. Zhou, J.B. Marroquin, M. Liu, S. Thomas, H.A. Coleman, D. Li, J.B. Fallon, M. Majumder, H.C. Parkington, J.S. Forsythe, Flexible neural recording electrodes based on reduced graphene oxide interfaces, Chem. Eng. J. 478 (2023) 147067, https://doi.org/10.1016/j.cej.2023.147067.
[22] U.S. Chio, E. Palovcak, A.A.A. Smith, H. Autzen, E.N. Muñoz, Z. Yu, F. Wang, D. A. Agard, J.P. Armache, G.J. Narlikar, Y. Cheng, Functionalized graphene-oxide grids enable high-resolution cryo-EM structures of the SNF2h-nucleosome complex without crosslinking, Nat. Commun. 15 (2024) 1–12, https://doi.org/10.1038/s41467-024-46178-y.
[23] V. Agrahari, P. Hiremath, Challenges associated and approaches for successful translation of nanomedicines into commercial products, Nanomedicine 12 (2017) 819–823, https://doi.org/10.2217/nnm-2017-0039.
[24] V.A. Rao, J.J. Kim, D.S. Patel, K. Rains, C.R. Estoll, A comprehensive scientific survey of excipients used in currently marketed, therapeutic biological drug products, Pharm. Res. 37 (2020) 200, https://doi.org/10.1007/s11095-020-02919-4.
[25] C.M. Zimmermann, L. Deßloch, D.C. Jürgens, P. Luciani, O.M. Merkel, Evaluation of the effects of storage conditions on spray-dried siRNA-LNPs before and after subsequent drying, Eur. J. Pharm. Biopharm. 193 (2023) 218–226, https://doi.org/10.1016/j.ejpb.2023.11.007.
[26] P. Sundaramurthi, R. Suryanarayanan, Trehalose crystallization during freeze-drying: implications on lyoprotection, J. Phys. Chem. Lett. 1 (2010) 510–514, https://doi.org/10.1021/jz900338m.
[27] B.J. Hong, O.C. Compton, Z. An, I. Eryazici, S.T. Nguyen, Successful stabilization of graphene oxide in electrolyte solutions: enhancement of biofunctionalization and cellular uptake, ACS Nano 6 (2012) 63–73, https://doi.org/10.1021/nn202355p.
[28] H. Huang, H. Park, J. Huang, Self-crosslinking of graphene oxide sheets by dehydration, Chem 8 (2022) 2432–2441, https://doi.org/10.1016/j.chempr.2022.05.016.
[29] L. Qiu, J.Z. Liu, S.L.Y. Chang, Y. Wu, D. Li, Biomimetic superelastic graphene-based cellular monoliths, Nat. Commun. 3 (2012) 1241, https://doi.org/10.1038/ncomms2251.
[30] A. Alazmi, O. El Tall, S. Rasul, M.N. Hedhili, S.P. Patole, P.M.F.J. Costa, A process to enhance the specific surface area and capacitance of hydrothermally reduced graphene oxide, Nanoscale 8 (2016) 17782–17787, https://doi.org/10.1039/C6NR04426C.
[31] Y. Shi, C. Li, L. Shen, N. Bao, Structure-dependent re-dispersibility of graphene oxide powders prepared by fast spray drying, Chin. J. Chem. Eng. 32 (2021) 485–492, https://doi.org/10.1016/j.cjche.2020.08.023.
[32] D. Parviz, S.D. Metzler, S. Das, F. Irin, M.J. Green, Tailored crumpling and unfolding of spray-dried pristine graphene and graphene oxide sheets, Small 11 (2015) 2661–2668, https://doi.org/10.1002/smll.201403466.
[33] J. Wang, X. Gao, Y. Wang, C. Gao, Novel graphene oxide sponge synthesized by freeze-drying process for the removal of 2,4,6-trichlorophenol, RSC Adv. 4 (2014) 57476–57482, https://doi.org/10.1039/C4RA09995H.
[34] Z. Xu, B. Zheng, J. Chen, C. Gao, Highly efficient synthesis of neat graphene nanoscrolls from graphene oxide by well-controlled lyophilization, Chem. Mater. 26 (2014) 6811–6818, https://doi.org/10.1021/cm503418h.
[35] J. Schmuck, W. Rondan, U. Reno, J. Vasquez, L. Regaldo, A.M. Gagneten, A. Champi, Lyophilized and sonicated graphene oxide and its nanoecotoxicity applications, Diam. Relat. Mater. 145 (2024) 111145, https://doi.org/10.1016/j.diamond.2024.111145.
[36] H. Hsein, C. Madi, V. Mazel, P. Tchoreloff, V. Busignies, Tableting properties of freeze-dried trehalose: physico-chemical and mechanical investigation, Int. J. Pharm. 648 (2023) 123598, https://doi.org/10.1016/j.ijpharm.2023.123598.
[37] M. Siri, M. Grasselli, S. del V. Alonso, Albumin-based nanoparticle trehalose lyophilisation stress-down to preserve structure/function and enhanced binding, J. Pharm. Biomed. Anal. 126 (2016) 66–74, https://doi.org/10.1016/j.jpba.2016.04.037.
[38] G. Degobert, D. Aydin, Lyophilization of nanocapsules: instability sources, formulation and process parameters, Pharmaceutics 13 (2021) 1112, https://doi.org/10.3390/pharmaceutics13081112.
[39] W. Abdelwahed, G. Degobert, H. Fessi, Investigation of nanocapsules stabilization by amorphous excipients during freeze-drying and storage, Eur. J. Pharm. Biopharm. 63 (2006) 87–94, https://doi.org/10.1016/j.ejpb.2006.01.015.
[40] K. Izutsu, S. Yoshioka, T. Terao, Decreased protein-stabilizing effects of cryoprotectants due to crystallization, Pharm. Res. 10 (1993) 1232–1237, https://doi.org/10.1023/a:1018988823116.
[41] J. Li, H. Wang, L. Wang, D. Yu, X. Zhang, Stabilization effects of saccharides in protein formulations: a review of sucrose, trehalose, cyclodextrins and dextrans, Eur. J. Pharmaceut. Sci. 192 (2024) 106625, https://doi.org/10.1016/j.ejps.2023.106625.
[42] S. Ohtake, Y.J. Wang, Trehalose: current use and future applications, J. Pharmacol. Sci. 100 (2011) 2020–2053, https://doi.org/10.1002/jps.22458.
[43] A. Richards, S. Krakowka, L. Dexter, H. Schmid, A.P. Wolterbeek, D. Waalkens-Berendsen, A. Shigoyuki, M. Kurimoto, Trehalose: a review of properties, history of use and human tolerance, and results of multiple safety studies, Food Chem. Toxicol. 40 (2002) 871–898, https://doi.org/10.1016/S0278-6915(02)00011-X.
[44] D. Vinciguerra, M.B. Gelb, H.D. Maynard, Synthesis and application of trehalose materials, JACS Au 2 (2022) 1561–1587, https://doi.org/10.1021/jacsau.2c00309.
[45] K.D. Roe, T.P. Labuza, Glass transition and crystallization of amorphous trehalose-sucrose mixtures, Int. J. Food Prop. 8 (2005) 559–574, https://doi.org/10.1080/10942910500269824.
[46] L. (Lucy) Chang, D. Shepherd, J. Sun, D. Ouellette, K.L. Grant, X. (Charlie) Tang, M. J. Pikal, Mechanism of protein stabilization by sugars during freeze-drying and storage: native structure preservation, specific interaction, and/or immobilization in a glassy matrix? J. Pharmacol. Sci. 94 (2005) 1427–1444, https://doi.org/10.1002/jps.20364.
[47] P. Fonte, S. Reis, B. Sarmento, Facts and evidences on the lyophilization of polymeric nanoparticles for drug delivery, J. Contr. Release 225 (2016) 75–86, https://doi.org/10.1016/j.jconrel.2016.01.034.
[48] A. Murray, P. Kilbride, M.I. Gibson, Trehalose in cryopreservation. Applications, mechanisms and intracellular delivery opportunities, RSC Med. Chem. 15 (2024) 2980–2995, https://doi.org/10.1039/D4MD00174E.
[49] R.G. Strickley, W.J. Lambert, A review of formulations of commercially available antibodies, J. Pharmacol. Sci. 110 (2021) 2590–2608.e56, https://doi.org/10.1016/j.xphs.2021.03.017.
[50] I. Ghosh, H. Gutka, M.E. Krause, R. Clemens, R.S. Kashi, A systematic review of commercial high concentration antibody drug products approved in the US: formulation composition, dosage form design and primary packaging considerations, mAbs 15 (2023), https://doi.org/10.1080/19420862.2023.2205540.
[51] W. Wang, Tolerability of hypertonic injectables, Int. J. Pharm. 490 (2015) 308–315, https://doi.org/10.1016/j.ijpharm.2015.05.069.
[52] T.M. Amis, J. Renukuntla, P.K. Bolla, B.A. Clark, Selection of cryoprotectant in lyophilization of progesterone-loaded stearic acid solid lipid nanoparticles, Pharmaceutics 12 (2020) 892, https://doi.org/10.3390/pharmaceutics12090892.
[53] L. Niu, J. Panyam, Freeze concentration-induced PLGA and polystyrene nanoparticle aggregation: imaging and rational design of lyoprotection, J. Contr. Release 248 (2017) 125–132, https://doi.org/10.1016/j.jconrel.2017.01.019.
[54] W.C. Luo, A. O'Reilly Beringhs, R. Kim, W. Zhang, S.M. Patel, R.H. Bogner, X. Lu, Impact of formulation on the quality and stability of freeze-dried nanoparticles, Eur. J. Pharm. Biopharm. 169 (2021) 256–267, https://doi.org/10.1016/j.ejpb.2021.10.014.
[55] S. Abdella, F. Abid, S.H. Youssef, S. Kim, F. Afinjuomo, C. Malinga, Y. Song, S. Garg, pH and its applications in targeted drug delivery, Drug Discov, Today Off. 28 (2023) 103414, https://doi.org/10.1016/j.drudis.2022.103414.
[56] I. Usach, R. Martinez, T. Festini, J.-E. Peris, Subcutaneous injection of drugs: literature review of factors influencing pain sensation at the injection site, Adv. Ther. 36 (2019) 2986–2996, https://doi.org/10.1007/s12325-019-01101-6.

[57] K.J. Sollanek, R.W. Kenefick, S.N. Cheuvront, Osmolality of commercially available oral rehydration solutions: impact of brand, storage time, and temperature, Nutrients 11 (2019) 1485, https://doi.org/10.3390/nu11071485.

[58] A. Duralliu, P. Matejtschuk, D.R. Williams, Humidity induced collapse in freeze dried cakes: a direct visualization study using DVS, Eur. J. Pharm. Biopharm. 127 (2018) 29–36, https://doi.org/10.1016/j.ejpb.2018.02.003.

[59] L. Rey, J. May, Freeze-Drying/Lyophilization of Pharmaceutical and Biological Products, third ed., CRC Press, 2016 https://doi.org/10.3109/9781439825761.